Draft version September 17, 2012
Preprint typeset using LaTeX style emulateapj v. 5/2/11

arXiv:1209.3037v1 [astro-ph.CO] 13 Sep 2012

THE SPECTRAL ENERGY DISTRIBUTIONS OF $Z \sim 8$ GALAXIES FROM THE IRAC ULTRA DEEP FIELDS: EMISSION LINES, STELLAR MASSES, AND SPECIFIC STAR FORMATION RATES AT 650 MYR [1]

I. Labbé[2], P. A. Oesch[3,4], R. J. Bouwens[2], G. D. Illingworth[3], D. Magee[3] V. González[3], C. M. Carollo[5], M. Franx[2], M. Trenti[6], P. G. van Dokkum[7] M. Stiavelli[8],

Draft version September 17, 2012

ABSTRACT

Using new ultradeep Spitzer/IRAC photometry from the IRAC Ultradeep Field program (IUDF), we investigate the stellar populations of a sample of 63 $Y-$dropout galaxy candidates at $z \sim 8$, only 650Myr after the Big Bang. The sources are selected from HST/ACS+WFC3/IR data over the Hubble Ultra Deep Field (HUDF), two HUDF parallel fields, and wide area data over the CANDELS/GOODS-South. The new Spitzer/IRAC data increase the exposure time in [3.6] and [4.5] to $\sim$ 120h over the HUDF reaching depths of ~ 28 (AB, 1σ). The improved depth and inclusion of brighter candidates result in direct $\geq 3\sigma$ IRAC detections of 20/63 sources (32%), of which 9 (14%) are detected at $\geq 5\sigma$. Stacking fainter galaxies to estimate average properties we find that the typical $L^*(z=8)$ galaxy has $H-[3.6] = 0.35 \pm 0.15$ and $[3.6]-[4.5] = 0.30 \pm 0.15$. These colors are significantly different from those of $z-$dropout galaxies at $z \sim 7$, observed only 130Myr later. The simplest explanation is that we witness strong rest-frame optical emission lines ([O III]$4959, 5007 + H\beta$) moving through the IRAC bandpasses with redshift. The presence of emission lines is further supported by evidence that $z \sim 8$ galaxies with *bluer* $J-H$ (rest-frame UV) show *redder* $[3.6]-[4.5]$ colors (rest-frame $B-V$). We can obtain a model independent estimate of the equivalent width by assuming that the average rest-frame spectrum is the same at both $z \sim 7$ and $z \sim 8$, finding $\mathrm{W}_{[OIII]4959,5007+H\beta} = 500^{+226}_{-164}$Å contributing ≈0.44 mag to [4.5] at $z \sim 8$. Correcting for this, the typical $L^*(z=8)$ galaxy has rest-frame color $U-V \approx 0.2$ (AB), mass-to-light ratios $M/L_{UV} \approx 0.07$, stellar mass $M \approx 1 \times 10^9\ M_\odot$, and specific star formation rate 5 Gyr^{-1}. The integrated stellar mass density (SMD) to $M_{UV,AB} < -18$ is $\rho^*(z=8) = 1.0^{+0.7}_{-0.5} \times 10^6\ M_\odot$ Mpc^{-3}.

Subject headings: galaxies: evolution — galaxies: high-redshift

1. INTRODUCTION

Deep imaging of high redshift $z > 6$ galaxies at mid-infrared wavelengths with the InfraRed Array Camera (IRAC; Fazio et al. 2004) on *Spitzer* has led to the surprising discovery that $z \geq 6$ galaxies have red $H-[3.6] \sim 0.5$ colors. This has been taken as evidence of substantial stellar masses $\sim 10^9 - 10^{10} M_\odot$ (Eyles et al. 2005; Yan et al. 2006; Stark et al. 2009) and stellar ages ($>$ 300Myr) (Labbé et al. 2006; González et al. 2010; Labbé et al. 2010a,b). Early studies also suggested that the specific star formation rate at fixed stellar mass was nearly flat at $3 < z < 8$, in apparent disagreement with the strongly increasing specific inflow rates of baryons predicted by galaxy formation models (e.g., Neistein & Dekel 2008; Davé et al. 2011, Weinmann et al. 2011).

A key uncertainty in the analysis of the photometry is how much rest-frame optical emission lines contribute to the broadband fluxes. If emission lines are very strong, then the stellar masses previously derived by fitting stellar population models without lines would be biased high, and the specific star formation rate (sSFR) would be biased low (cf., Labbé et al. 2010b, Schaerer & de Barros 2010). To address this issue, it is possible to include emission lines in the stellar population models (e.g., Schaerer et al. 2010, 2012, de Barros et al. 2012, Yan et al. 2012). However, the correct implementation is not certain and no direct spectroscopic measurements in the rest-frame optical exist at $z > 4$ to test the models. Alternative empirical approaches have also been undertaken: e.g., by extrapolating existing trends over $0 < z < 2$ to $z = 8$ (Fumagalli et al. 2012), by looking for excess flux in [3.6]$-$band at $z \sim 4.5$, using [4.5] as a control filter, (e.g. Shim et al. 2011, Stark et al. 2012), or by comparing the observed IRAC colors over a range of redshifts (Gonzalez et al. 2012). Nevertheless, the current situation is that the contribution of emission lines over $4 < z < 8$ is still poorly quantified.

Although challenging, it would be particularly interest-

---

[1] Based on observations made with the NASA/ESA Hubble Space Telescope, which is operated by the Association of Universities for Research in Astronomy, Inc., under NASA contract NAS 5-26555. These observations are associated with programs #11563, 9797. Based on observations with the *Spitzer Space Telescope*, which is operated by the Jet Propulsion Laboratory, California Institute of Technology under NASA contract 1407. Support for this work was provided by NASA through contract 125790 issued by JPL/Caltech. Based on service mode observations collected at the European Southern Observatory, Paranal, Chile (ESO Program 073.A-0764A). Based on data gathered with the 6.5 meter Magellan Telescopes located at Las Campanas Observatory, Chile.

[2] Leiden Observatory, Leiden University, NL-2300 RA Leiden, Netherlands

[5] UCO/Lick Observatory, University of California, Santa Cruz, CA 95064

[4] Hubble Fellow

[5] Institute for Astronomy, ETH Zurich, 8092 Zurich, Switzerland

[6] Institute of Astronomy, University of Cambridge, Cambridge, United Kingdom

[7] Department of Astronomy, Yale University, New Haven, CT 06520

[8] Space Telescope Science Institute, Baltimore, MD 21218, United States

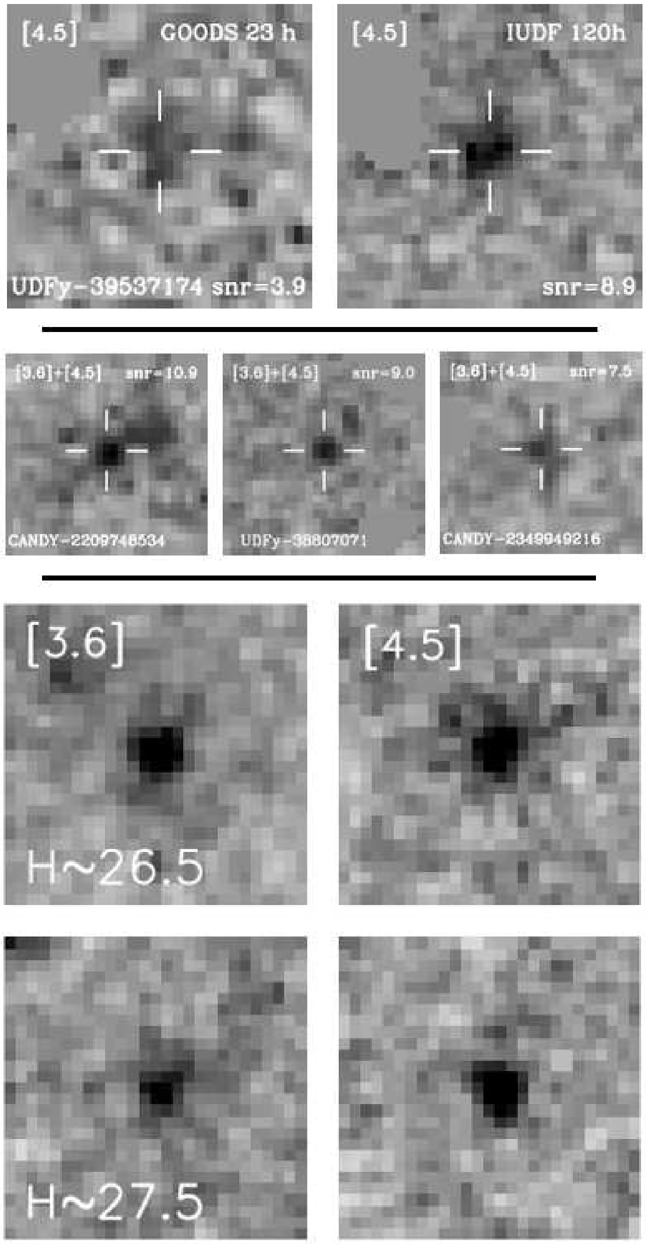

Figure 1. (*top panels*) A comparison of Spitzer/IRAC [4.5] band images between GOODS (23h exposure time) and the new IUDF10 observations (120h) for $Y_{105}-$dropout galaxy UDFy-3953714 (Bouwens et al. 2011a) at $z \sim 8$. Nearby foreground sources have been subtracted. With the new IUDF10 IRAC data the object is clearly detected, even in the shallower IRAC [4.5] micron band. (*middle panels*) Summed $[3.6] + [4.5]$ micron images of several IRAC detected $Y_{105}-$dropouts from our sample. (*bottom panels*) Median stacked IRAC images of $z \sim 8$ Y-dropout sources, grouped in $\sim 1-$mag bins centered on $H_{160} \approx 26.5, 27.5$, containing 10 and 23 galaxies, respectively. Importantly, the stacks show significant detections at [3.6], which at $z \sim 8$ is not affected by strong emission lines. Image panels are shown in inverted grayscale and are $10'' \times 10''$.

ing to extend these measurements to $z \sim 8$. The highest redshifts provide better leverage to constrain the evolution of emission line strengths between $4 < z < 8$. Redshift $z \sim 8$ also provides an opportunity to test for the strength of the emission lines, since the [3.6] filter is unaffected by strong lines, with the strongest line [O III] isolated to the [4.5] filter.

In this Letter, we use the largest sample of $z \sim 8$ galaxy candidates in combination with newly acquired ultradeep IRAC data from the IRAC Ultra Deep Field program (IUDF; PI Labbé) to study their colors, SEDs, and the contribution of emission lines, and to derive emission line corrected stellar masses and specific star formation rates. Throughout this paper, we assume an $\Omega_M = 0.3, \Omega_\Lambda = 0.7$ cosmology with $H_0 = 70$ km s^{-1}Mpc^{-1}. Magnitudes are in the AB photometric system (Oke & Gunn 1983).

2. DATA

2.1. *Observations*

The data analyzed here consist of ultradeep WFC3/IR imaging from the HUDF09 program (GO 11563: PI Illingworth) over the HUDF and two nearby fields HUDF09-1 and HUDF09-2, supplemented with deep WFC3/IR data observations from the Early Release Science program (GO 11359: PI O'Connell) and the Multi-Cycle Treasury program CANDELS (PI: Faber/Ferguson; Grogin et al. 2011; Koekemoer et al. 2011) over the GOODS-South.

We use new ultradeep Spitzer/IRAC imaging from the IRAC Ultradeep Field program (IUDF; PI Labbé), a 262 hour Spitzer warm mission program at [3.6] and [4.5] micron (Labbé et al. in preparation). This survey increases the exposure time over the HUDF, HUDF09-1 and HUDF09-2 fields from $12-46$ hours to $\sim$120 hours, $\sim$50 hours, and $80-120$ hours, respectively. For the wider GOODS area we use the $23-46$ hour deep IRAC coverage of GOODS (M. Dickinson et al. in preparation).

Our primary sample consists of 60 $Y-$dropout galaxies at $z \sim 8$ selected by Bouwens et al. (2011a) over the HUDF09 and ERS fields and 16 brighter $Y-$dropouts selected by Oesch et al. (2012) over the CANDELS GOODS-South area.

We derive new IRAC photometry of all 76 sources following the procedure of Labbé et al. (2010a,b). Briefly, we subtract nearby foreground sources based on their HST image profiles and determine local backgrounds (see e.g, Gonzalez et al 2011). Then we perform aperture photometry through $2''$ diameter apertures on the cleaned images. Details of the photometry are presented in Labbé et al. (in preparation). We exclude 13 sources for which clean subtraction was not possible due to proximity to very bright foreground galaxies, leaving a final sample of 63 $Y-$dropouts.

Figure 1 presents image stamps of IRAC$-$detected $Y-$dropout galaxies. A direct comparison to earlier GOODS observations demonstrates the clear improvement in sensitivity with the new ultradeep IUDF IRAC data over the HUDF. To include fainter, IRAC undetected, galaxies in the analysis we split the $z \sim 8$ sample into various subsamples, and stack $15'' \times 15''$ image stamps centered on the sources. The bottom panels show that detections are also evident for fainter galaxies in the stacks. We measure flux densities through $2''$ diameter apertures on each stack, subtract any residual background in a concentric annulus at $5'' < r < 7.5''$. We compare between average and median stacks to make sure that the measurements are not driven by outliers. The uncertainties are determined by bootstrapping. We correct the flux for light outside the aperture using pro-

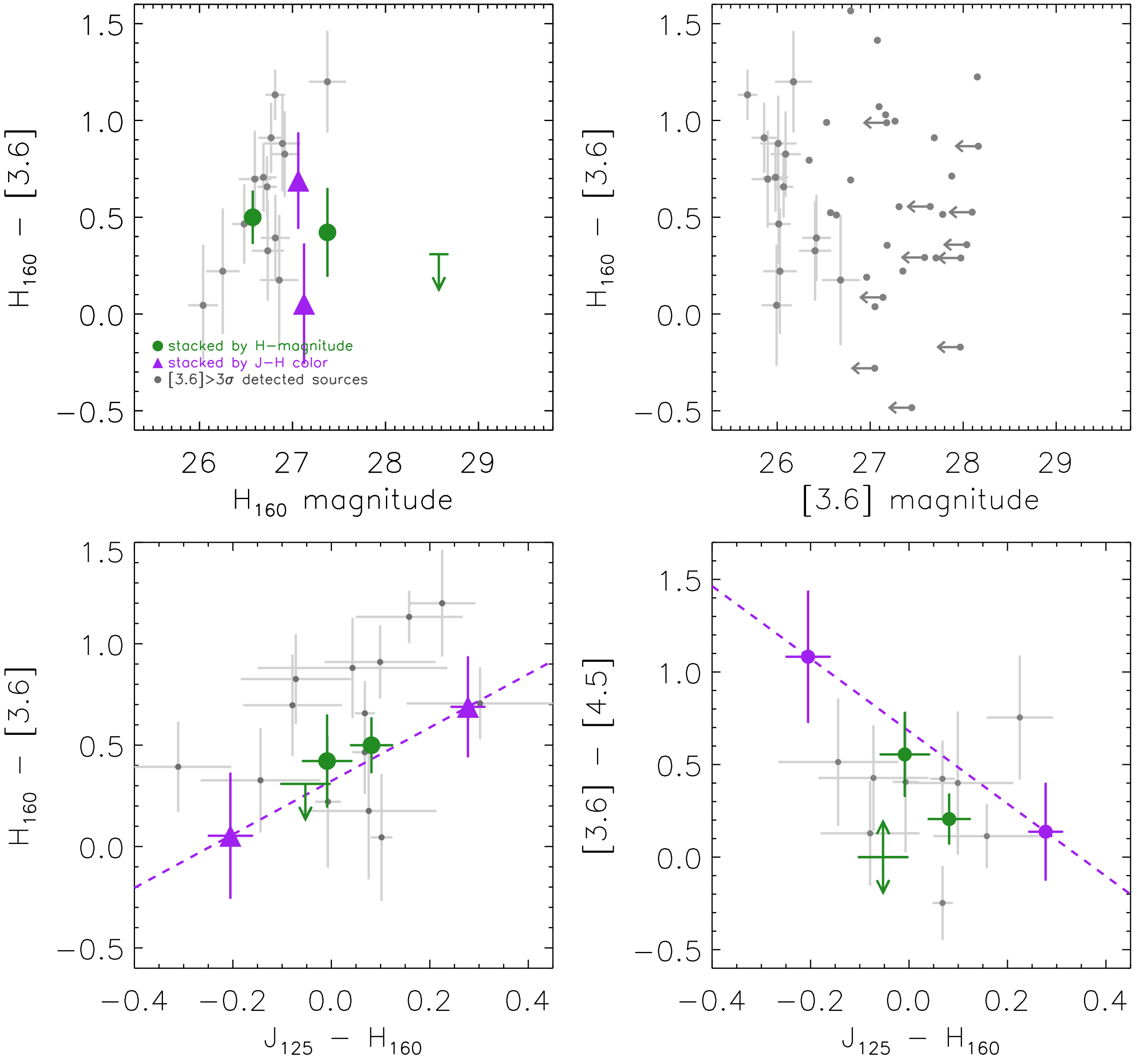

Figure 2. (*top left panel*) The $H_{160} - [3.6]$ versus H_{160} diagram of the $z \sim 8$ sources in our fields. Galaxies directly detected at $> 3\sigma$ in [3.6] are shown by gray points. Stacked measurements in three bins of luminosity are shown in green and stacks in two bins of $J_{125} - H_{160}$ colors are shown in purple. A mild trend with $H-$magnitude may exist, but deeper data is needed to extend the analysis to $H_{160} \sim 28.5$. Stronger trends are found versus $J_{125} - H_{160}$ color. (*top right panel*) The observed $H - [3.6]$ versus [3.6] magnitude. Sources with SNR([3.6]) $< 3\sigma$ are now also shown (upper limits are 1σ). The deepest data over the HUDF reaches ~ 28 mag AB (1σ). (*lower left panel*) The observed $H - [3.6]$ versus $J_{125} - H_{160}$ (*middle panel*) shows redder $H - [3.6]$ color towards redder $J_{125} - H_{160}$ color. In contrast, galaxies *bluer* in $J_{125} - H_{160}$ produce *redder* $[3.6] - [4.5]$ colors (rest-frame $B_{4000} - V_{5000}$; *lower right panel*). Such joint correlations can not be produced by dust or changes in the stellar continuum alone, but likely require the presence of strong optical emission lines contributing to the $[4.5]-$band at $z \sim 8$.

files derived from nearby stars (typically 2.4× in [3.6] and 2.5× in [4.5]).

3. OBSERVED PROPERTIES

3.1. *Observed colors*

We first present key color−magnitude and color−color relations which suggest that the combined WFC3/IR and Spitzer/IRAC colors contain important diagnostic information about $z \sim 8$ galaxies. Figure 2 (*left panel*) shows the $H_{160} - [3.6]$ versus H_{160} color-magnitude diagram. The improved IRAC depth and inclusion of brighter candidates result in a direct detection with $\geq 3\sigma$ in either [3.6] or [4.5] of 20/63 sources (32%), of which 9 (14%) are detected at $\geq 5\sigma$. To a bright magnitude limit of $H_{160} < 27.0$ all 14 sources are detected in the [3.6] band, allowing us to estimate the scatter in the properties of bright $z \sim 8$ galaxies. The bright subsample shows an intrinsic scatter of $\sigma(H - [3.6]) = 0.6 \pm 0.2$ (determined by bootstrapping and subtracting the median photometric uncertainty in quadrature).

To study trends in the average colors, we split the sample in two ways: in three magnitude bins centered on $H \sim 26.5$, $H \sim 27.5$, and $H \sim 28.5$ (containing 10, 23, and 30 galaxies) and in two color bins representing the highest and lowest tertile of the $J_{125} - H_{160}$ distribution (containing 10 galaxies each). For the color bins we limit ourselves to the brightest half ($H_{160} < 27.8$) of the sample to ensure sufficient SNR in IRAC. The sources are significantly detected in all stacks, except the faintest $H \sim 28.5$ stack.

Figure 2 shows that a mild trend of bluer $H_{160} - [3.6]$ colors towards fainter H_{160} magnitudes may exist, although deeper IRAC are required to extend the baseline to the faintest magnitudes > 28 AB. A clear trend in the data is that sources with redder $J_{125} - H_{160}$ colors also have redder $H_{160} - [3.6]$ (rest-frame $U_{1700} - B_{4000}$). In contrast, galaxies *bluer* in $J_{125} - H_{160}$ produce *redder* $[3.6] - [4.5]$ colors (rest-frame $B_{4000} - V_{5000}$).

The anticorrelation between $J_{125} - H_{160}$ and $[3.6] - [4.5]$ cannot be produced by changes in the stellar continuum (e.g., with metallicity, age) or dust, since they would produce the same trend in the rest-frame UV as in the rest-frame optical. However, young star forming galaxies at high redshift are expected to show emission lines, in particular [O III]4959, 5007 and $H\beta$, which fall in the middle of the [4.5]−band at $z = 8$. If those emission lines are very strong in the bluest galaxies (e.g., because of younger ages and/or lower metallicity), then they could produce redder $[3.6] - [4.5]$ colors. Alternatively, galaxies with rest-frame optical emission lines might have blue $J_{125} - H_{160}$ colors due to Lyα emission contributing to the J_{125}−band.

If the sole cause of the trend towards redder $[3.6] - [4.5]$ colors is line emission contributing to [4.5] then Figure 2 suggests that the amount may be substantial (~ 0.5 mag for $H \sim 27.5$ and possibly ~ 1 mag for the bluest $J - H \sim -0.2$ galaxies).

3.2. *Rest-frame optical emission lines*

While the color trends suggest a strong contribution of emission lines, to determine the absolute amount requires disentangling the contributions of stellar continuum and emission lines, which is not possible from broadband photometry at $z \sim 8$ alone. Here we attempt to circumvent this limitation by using the joint information of the IRAC colors at two adjacent redshifts, combining our measurements at $z \sim 8$ with previous results at $z \sim 7$ (Labbé et al. 2010b).

Tantalizingly, Figure 3 (*right*) shows that observed $H_{160} - [3.6]$ versus $[3.6] - [4.5]$ colors of L^* galaxies at $z \sim 8$ are markedly different from those at $z \sim 7$, only 130Myr later. Most significantly, the $[3.6] - [4.5] \approx 0.3$ colors at $z \sim 8$ are 0.6 mag redder than those at $z \sim 7$, while the $H - [3.6]$ colors are 0.3 mag bluer. Changes in stellar population age and/or dust can not produce such differences. However, strong optical emission lines can naturally reproduce the observed change, as $[\mathrm{O\ III}]_{4959,5007}$ and $H\beta$ move from [4.5] at $z \sim 8$ into [3.6] at ~ 7.

With the reasonable assumption that the average rest-frame spectrum is the same at both $z \sim 8$ and $z \sim 7$, we can solve for the EW of these emission lines. A naive linear fit to the median colors assuming a fixed redshift $z = 6.8$ and $z = 7.8$ for the samples gives an equivalent width $W_{[OIII]4959,5007+H\beta} = 280\mathring{A}$. Taking into account the redshift selection functions of Oesch et al. (2012) and Bouwens et al. (2011a) produces $W_{[OIII]4959,5007+H\beta} = 410\text{Å}$. The increase is due to the emission lines contaminating both [3.6] and [4.5] for the redshift distribution of the $z \sim 7$ sample. Including lines such as Hα and [O II]) (using the relative strengths tabulated by Anders & Fritze-v.Alvensleben 2003 for sub-solar $0.2Z_{\odot}$) results in $W_{[OIII]4959,5007+H\beta} = 500\text{Å}\pm160\text{Å}$, corresponding to a contribution of 0.44 mag to [4.5] at $z \sim 8$.

Note that this empirical estimate is model independent and the fit only has one free parameter: the combined equivalent width of the strong emission lines. The main systematic uncertainty is the redshift selection function for the $z \sim 7$ sample. To evaluate its impact we shift the central redshift of the $z \sim 7$ distribution by up to $\Delta z = 0.3$ in either direction finding a range $W_{[OIII]4959,5007+H\beta} = 460 - 660\text{Å}$. We add this systematic uncertainty in quadrature to the photometric errors arriving at $W_{[OIII]4959,5007+H\beta} = 500\text{Å}^{+226}_{-164}\text{Å}$.

Combining this estimate with the observed anticorrelation between $[3.6] - [4.5]$ and $J_{125} - H_{160}$ colors shown in Figure 2 we can also calculate a correction on the emission line contribution as a function of $J_{125} - H_{160}$ color:

$$\Delta[4.5]_{EL} = 0.4 - 2.0\ (J - H) > 0 \qquad (z \sim 8) \tag{1}$$

The correction ranges from $0 < \Delta[4.5]_{EL} < 0.9$ mag for $0.25 < J - H < -0.25$, corresponding to a total equivalent width of $0 < W < 1100\mathring{A}$. Note that including the effects of dust reddening or redshift (e.g. when the Lyman break starts entering J_{125}), would imply larger corrections for a given $\Delta(J_{125} - H_{160})$.

3.3. *Spectral Energy Distributions*

Figure 4 (*left panel*) shows the spectral energy distributions from the stacked HST/ACS, HST/WFC3, and Spitzer/IRAC fluxes, binned by H_{160}−band magnitude. We show the original measurements, but also the emission line corrected [4.5] magnitude using the empirical relation $\Delta[4.5]_{EL}$ from Eq. 1. Both the average $J_{125} - H_{160}$

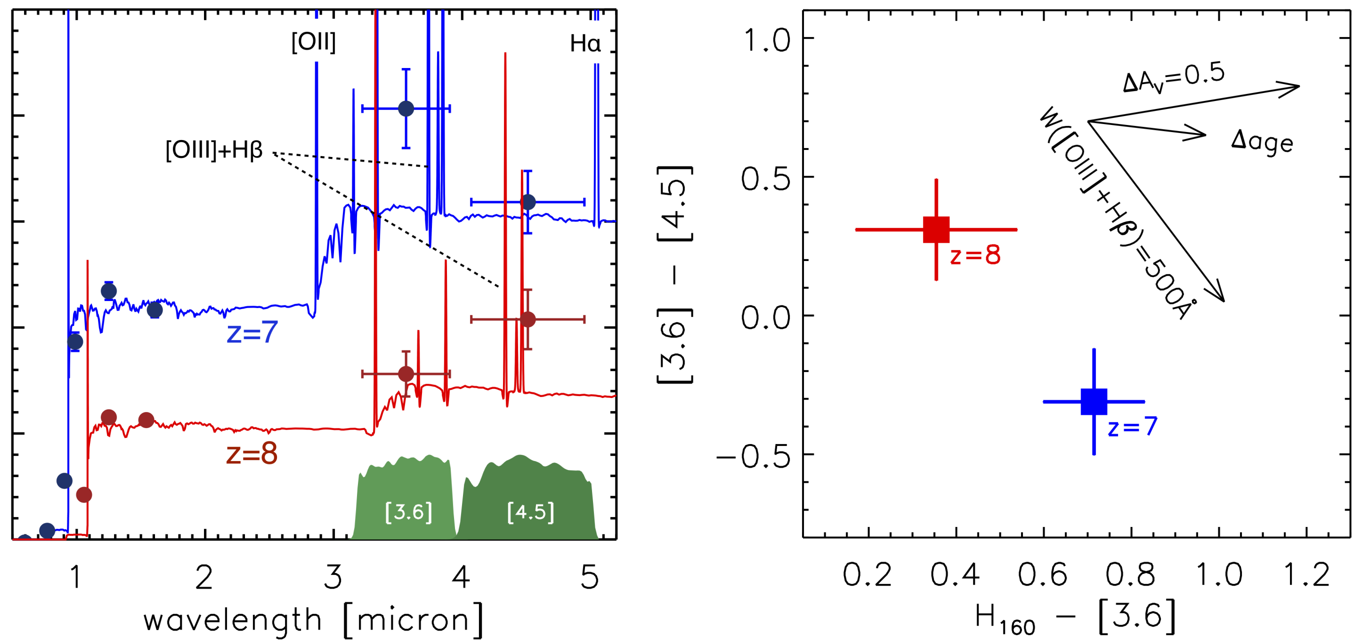

Figure 3. (*left panel*) A comparison of the average SED at $z \sim 8$ to the average SED at $z \sim 7$ (from Labbé et al. 2010b). The SEDs are offset vertically for clarity. The SED shapes are substantially different, despite the short time elapsed between these epochs (only 130Myr). (*right panel*) Focusing on the $H_{160} - [3.6]$ versus $[3.6] - [4.5]$ colors we find that the $[3.6] - [4.5]$ colors become ≈ 0.6 mag bluer from $z \sim 8$ to $z \sim 7$ while the $H - [3.6]$ colors become ≈ 0.3 mag redder. The arrows show the effect of increasing dust obscuration by $\Delta A_V = 0.5$ between the two epochs or changing the stellar population age by 130Myr (assuming CSF since $z = 10$): neither can reproduce the observed changes. However, strong optical emission lines naturally produces the required trend, primarily reflecting [O III]$_{4959,5007}$ and $H\beta$ moving from [4.5] at $z \sim 8$ into [3.6] at $z \sim 7$. The predicted change with redshift of a contribution of equivalent width $W_{[OIII]4959,5007+H\beta} = 500\text{Å}$ is shown.

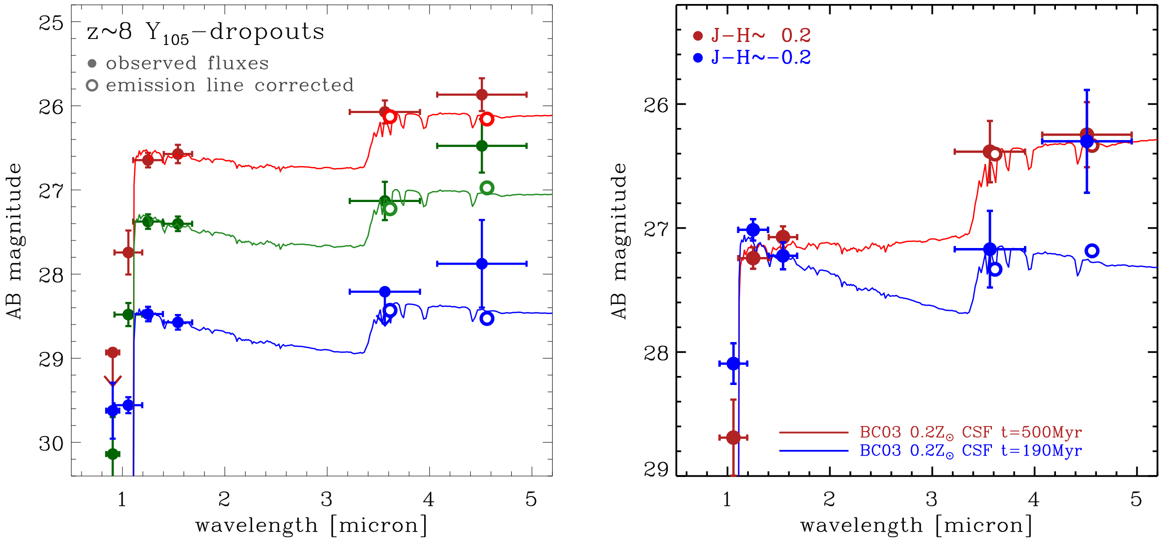

Figure 4. (*left panel*) Spectral energy distributions of $z \sim 8$ galaxies from the stacked HST/ACS, HST/WFC3, and Spitzer/IRAC fluxes, binned by H_{160}−band magnitude. Upper limits are 2σ. The SEDs show a mild trend of bluer shapes towards fainter magnitudes. A flux excess at [4.5] is visible at all magnitudes, likely due to strong [O III]4959, 5007 and $H\beta$ emission. IRAC [4.5] magnitudes corrected for emission lines using our empirical description are shown by open circles (with a slight offset in wavelength). The IRAC [3.6] band requires a smaller correction due to the contribution of [O II]3727. Solid lines show stellar population models fits to the corrected SEDs using BC03 models and Calzetti et al. (2000) dust. (*right panel*) at fixed $H \sim 27$ magnitude the galaxy sample shows strong variation with $J_{125} - H_{160}$ (rest-frame far-UV), such that blue $J - H$ and $H - [3.6]$ show the same trends, whereas the $[3.6] - [4.5]$ shows the opposite behavior with the bluest $J - H$ showing the reddest $H - [3.6]$.

and $H_{160} - [3.6]$ colors become somewhat bluer towards fainter magnitudes, possibly caused by lower dust obscuration, lower metallicity, and/or younger stellar population ages.

More dramatic differences can be seen as a function of $J_{125} - H_{160}$ color for galaxies brighter than $H_{160} \leq 27.8$ (half the sample). Figure 4 (*right panel*) shows the stacked SEDs of the bluest and reddest tertile of the sample. As already evident from the observed colors in Fig. 2, the $J-H$ and $H-[3.6]$ show the same trends, whereas the $[3.6] - [4.5]$ shows the opposite behavior with the bluest $J - H$ showing the reddest $[3.6] - [4.5]$. The empirical emission line correction brings the colors in agreement with those expected from the $H - [3.6]$ colors.

4. STELLAR POPULATIONS

Stellar masses and sSFRs are derived by fitting Bruzual & Charlot (2003, BC03) stellar populations synthesis models with a Salpeter (1955) initial mass function (IMF) between $0.1 - 100$ $M_\odot$ to the emission line corrected SEDs using the χ^2-fitting code FAST (Kriek et al. 2009). We assume a metallicity of 0.2 $Z_\odot$ (Erb et al. 2006; Maiolino et al. 2008) and a constant star formation history (CSF).

The solid lines in Fig. 4 show the best fits to the emission line corrected SEDs. The average galaxies show a range of masses from $M = 5 \times 10^9 M_\odot$ in the brightest $H \sim 26.5$ bin to $M = 3 \times 10^8 M_\odot$ in the faintest bin $H \sim 28.5$. The typical $L*(z = 8)$ galaxy (corresponding to $H \sim 27.3$) has a median rest-frame color $U - V \sim 0.2$ (stellar continuum only), mass-to-light ratios $M/L_{UV,1500} = 0.07$ and $M/L_V = 0.15$, and a stellar mass $M \approx 1 \times 10^9$ $M_\odot$. Assuming CSF, the best fit age $t = 230$Myr and the sSFR is 5 Gyr^{-1}. The mass-to-light ratios would have been ~ 0.3 dex higher and the sSFR ~ 0.3 dex lower if emission lines had not been corrected.

At fixed $H \sim 27$ mag the sample exhibits significant variation in colors and mass-to-light ratios, with the reddest tertile in $J_{125} - H_{160}$ having $M/L_{UV,1500} = 0.25$ and the bluest tertile having $M/L_{UV,1500} = 0.035$. This implies that $UV-$selected galaxies at very early times already show ×7 mass-to-light ratio variations at fixed $H_{160}-$band magnitude, which may introduce selection effects if unaccounted for.

Following the approach of González et al. (2012), we derive integrated stellar mass densities to faint limits at $z \sim 8$ by multiplying the stepwise $UV-$luminosity function (Bouwens et al. 2011a; Oesch et al. 2012) by the mean M/L ratios derived for the $z \sim 8$ sample at $H = 26.5, 27.5$, and 28.5. Integrating to $M_{UV,AB} = -18$ yields $\rho^*(z = 8) = 1.0^{+0.7}_{-0.5} \times 10^6$ $M_\odot$ Mpc^{-3}. These values are 0.3 dex lower than would have been derived without correcting for emission lines.

5. DISCUSSION

This paper presents new ultradeep IRAC data from the IUDF program (120 hours in [3.6] and [4.5] over the HUDF) in combination with a large sample of 63 $Y_{105}-$dropout galaxies at $z \sim 8$ to study average HST/WFC3 and Spitzer/IRAC SEDs, the effect of emission lines, and their impact on stellar population model fits.

The most impressive result is the direct detection of $z \sim 8$ galaxies by Spitzer/IRAC, without signs of a hard "confusion limit", and the ability for the first time to determine detailed systematic rest-frame $U-V$ color trends and color scatter at $z \sim 8$. This is a stunning reminder of the enduring capabilities of Spitzer, currently in its post cryogenic ("warm") mission. The robust determinations of stellar masses of the brightest individual galaxies provide evidence for the existence of massive $> 3 \times 10^9$ $M_\odot$ galaxies with relatively red colors already existing at very early times.

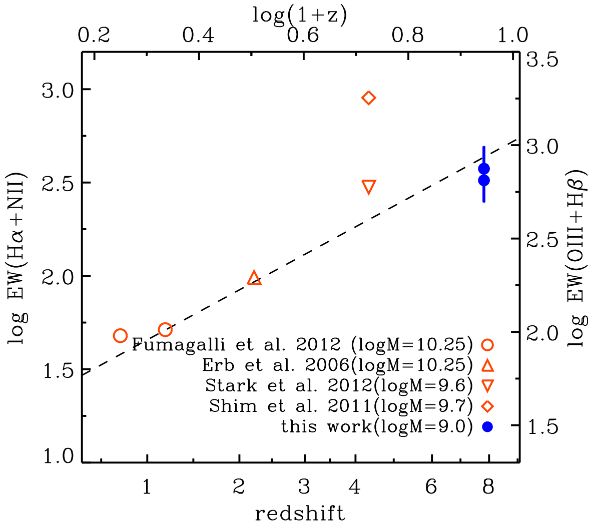

Figure 5. Comparison of the observed emission line EW with redshift. Red points indicate estimates of the mean $H\alpha$+[NII] EW with redshift, using either near-infrared spectra (Fumagalli et al. 2012, Erb et al. 2006) or emission line strengths inferred from excess emission in the IRAC [3.6] filter of spectroscopically confirmed galaxies at $z \sim 4 - 5$. The broadband derived $[OIII] + H\beta$ EW at $z \sim 8$ from this paper are shown by the blue solid symbols. They are placed on the same scale assuming the relative emission line strengths tabulated by Anders & Fritze-v.Alvensleben (2003) in the case of sub-Solar $0.2Z_\odot$ (lower value) and Solar (higher value), respectively. The dashed line shows the EW evolution $\propto (1+z)^{1.8}$ derived by Fumagalli et al. (2012) for galaxies with stellar mass $10.0 < \log(M/M\odot) < 10.5$ at $0 < z < 2$ extrapolated to $z = 8$. Although the data are too heterogeneous to allow direct comparisons (different techniques, different stellar mass ranges), the $z \sim 8$ point provides additional evidence for an increasing contribution of emission lines towards higher redshifts.

We empirically derive an emission line contribution at $z \sim 8$ with EW $W_{[OIII]4959,5007+H\beta} \sim 500$Å. To place this in context, we compare to recent estimates from other surveys (shown in Figure 5). While direct comparisons are difficult at this point due to different techniques and different stellar mass ranges probed by the surveys, our results are consistent with the picture of an increasingly prominent contribution of emission lines towards high redshift. It is interesting to note that the EWs at $z \sim 8$ are in a similar range as reported by Stark et al. (2012) and lower than those of Shim et al. (2011) at $z \sim 4 - 5$, which may suggest that the EW is not increasing rapidly over this range.

Our results confirm that emission lines cannot be ignored when deriving stellar masses and ages at high redshift. Fitting stellar population models to the emission line corrected SEDs, we find for the typical $L^*(z = 8)$ galaxy a stellar mass of $\sim 1 \times 10^9 M_\odot$ and a sSFR$\sim$ 5 Gyr^{-1}. These values are a factor ~ 2 lower and higher respectively than would have been derived if emission lines had not been considered. The sSFR at $z \sim 8$ are a factor of ~ 2.5 higher than at $z = 2 - 3$ (Reddy et al. 2012), consistent with the moderate evolution of the SSFR $z \propto (1+z)^{0.9}$ derived by Gonzalez et al. (2012) over $1 < z < 6$ and Stark et al. (2012; in the case of constant emission line EW at $4 < z < 7$), but somewhat slower than the strong evolution derived by Fumagalli et al. (2012). While accounting for the contribution of emission lines reduces the tension between the observations and predictions of the evolution of the sSFR from simulations, the increasing baryonic mass inflow rates $\propto (1+z)^{2.3}$ predicted by galaxy formation models (e.g., Neistein & Dekel 2008; Davé et al. 2011, Weinmann et al. 2011) still appear well in excess of the sSFR rate evolution inferred from observations.

Obviously, a huge leap in the determination of the properties of galaxies at these redshifts will be made possible by the arrival of JWST. But in the mean time wider and still deeper future IRAC observations will continue to provide valuable insight into the properties of the $z \sim 8$ population, with emerging detections of $z = 9$ (e.g., Zheng et al. 2012) and perhaps $z = 10$ galaxies probably not far behind.

We are grateful to Jarle Brinchmann, Steve Finkelstein, Casey Papovich, Dan Stark, Simone Weinmann for helpful discussions. Support for this work was provided by NASA through Hubble Fellowship grant HF-51278.01. This work has further been supported by NASA grant HST-GO-11563.01. We also acknowledge funding from ERC grant HIGHZ no. 227749.

Facilities: Spitzer (IRAC), HST (WFC3/IR)

REFERENCES

Anders, P., & Fritze-v. Alvensleben, U. 2003, A&A, 401, 1063
Bouwens, R. J., Illingworth, G. D., Franx, M., & Ford, H. 2008, ApJ, 686, 230
Bouwens, R. J., et al. 2010, ApJ, 709, L133
Bouwens, R. J., et al. 2010, ApJ, 708, L69
—. 2011, ApJ, 737, 90
Bouwens, R. J., Illingworth, G. D., Oesch, P. A., et al. 2012, ApJ, 754, 83
Bruzual, G. & Charlot, S. 2003, MNRAS, 344, 1000 (BC03)
Calzetti, D., et al. 2000, ApJ, 533, 682
Davé, R. 2008, MNRAS, 385, 147
de Barros, S., Schaerer, D., & Stark, D. P. 2012, arXiv:1207.3663
Erb, D. K., Shapley, A. E., Pettini, M., Steidel, C. C., Reddy, N. A., & Adelberger, K. L. 2006, ApJ, 644, 813
Eyles, L. P., et al. 2005, MNRAS, 364, 443
Fazio, G. G., et al. 2004, ApJS, 154, 10
Fumagalli, M., Patel, S., Franx, M., et al. 2012, arXiv:1206.2645
González, V., Labbé, I., Bouwens, R. J., Illingworth, G., Franx, M., Kriek, M., & Brammer, G. B. 2010, ApJ, 713, 115
González, V., Bouwens, R. J., Labbé, I., et al. 2012, ApJ, 755, 148
Gonzalez, V., Bouwens, R., llingworth, G., et al. 2012, arXiv:1208.4362
Kriek, M., van Dokkum, P. G., Labbé, I., Franx, M., Illingworth, G. D., Marchesini, D., & Quadri, R. F. 2009, ApJ, 700, 221
Labbé, I., et al. 2005, ApJ, 624, L81
Labbé, I., Bouwens, R., Illingworth, G. D., & Franx, M. 2006, ApJ, 649, L67
Labbé, I., et al. 2010, ApJ, 708, L26
Labbé, I., et al. 2010, ApJ, 716, L103
Maiolino, R., Nagao, T., Grazian, A., et al. 2008, A&A, 488, 463
Neistein, E., & Dekel, A. 2008, MNRAS, 383, 615
Oke, J. B., & Gunn, J. E. 1983, ApJ, 266, 713
Oesch, P. A., et al. 2009a, ApJ, 690, 1350
Oesch, P. A., et al. 2010, ApJ, 709, L16
Oesch, P. A., Bouwens, R. J., Illingworth, G. D., et al. 2012, ApJ accepted, arXiv:1201.0755
Reddy, N. A., Pettini, M., Steidel, C. C., et al. 2012, ApJ, 754, 25
Salpeter, E. E. 1955, ApJ, 121, 161
Schaerer, D., & de Barros, S. 2010, A&A, 515, A73
Schaerer, D., de Barros, S., & Sklias, P. 2012, arXiv:1207.3074
Shim, H., Chary, R.-R., Dickinson, M., et al. 2011, ApJ, 738, 69
Stark, D. P., Ellis, R. S., Bunker, A., Bundy, K., Targett, T., Benson, A., & Lacy, M. 2009, ApJ, 697, 1493
Stark, D. P., Schenker, M. A., Ellis, R. S., et al. 2012, arXiv:1208.3529
Yan, H., Dickinson, M., Giavalisco, M., Stern, D., Eisenhardt, P. R. M., & Ferguson, H. C. 2006, ApJ, 651, 24
Yan, H., Finkelstein, S. L., Huang, K.-H., et al. 2011, arXiv:1112.6406
Weinmann, S. M., Neistein, E., & Dekel, A. 2011, MNRAS, 417, 2737
Zheng, W., Postman, M., Zitrin, A., et al. 2012, arXiv:1204.2305